

Article

# Computational Discovery of New Feasible Crystal Structures in $\text{Ce}_3\text{O}_3\text{N}$

Jelena Zagorac <sup>1,2,\*</sup>, Johann Christian Schön <sup>3</sup>, Branko Matović <sup>1,2</sup>, Milan Pejić <sup>1,2</sup>, Marija Prekajski Đorđević <sup>1,2</sup> and Dejan Zagorac <sup>1,2</sup>

<sup>1</sup> Institute of Nuclear Sciences Vinča, Materials Science Laboratory, Belgrade University, 11000 Belgrade, Serbia; mato@vinca.rs (B.M.); milan.pejic@yahoo.com (M.P.); prekajski2@gmail.com (M.P.D.); dzagorac@vinca.rs (D.Z.)

<sup>2</sup> Center for Synthesis, Processing and Characterization of Materials for Application in the Extreme Conditions-CextremeLab, 11000 Belgrade, Serbia

<sup>3</sup> Max Planck Institute for Solid State Research, Heisenbergstr. 1, 70569 Stuttgart, Germany; c.schoen@fkf.mpg.de

\* Correspondence: jelena@vinca.rs

**Abstract:** Oxynitrides of cerium are expected to have many useful properties but have not been synthesized so far. We identified possible modifications of a not-yet-synthesized  $\text{Ce}_3\text{O}_3\text{N}$  compound, combining global search (GS) and data mining (DM) methods. Employing empirical potentials, structure candidates were obtained via global optimization on the energy landscape of  $\text{Ce}_3\text{O}_3\text{N}$  for different pressure values. Furthermore, additional feasible structure candidates were found using data mining of the ICSD database. The most promising structure candidates obtained were locally optimized at the *ab initio* level, and their E(V) curves were computed. The structure lowest in total energy,  $\text{Ce}_3\text{O}_3\text{N}$ -DM1, was found via local optimization starting from a data mining candidate and should be thermodynamically metastable up to high pressures.

**Keywords:** oxynitrides; global optimization; data mining; *ab initio*



**Citation:** Zagorac, J.; Schön, J.C.; Matović, B.; Pejić, M.; Prekajski Đorđević, M.; Zagorac, D.

Computational Discovery of New Feasible Crystal Structures in  $\text{Ce}_3\text{O}_3\text{N}$ . *Crystals* **2023**, *13*, 774. <https://doi.org/10.3390/cryst13050774>

Academic Editors: Saskia Schimmel and Natasha Dropka

Received: 3 April 2023

Revised: 25 April 2023

Accepted: 4 May 2023

Published: 6 May 2023



**Copyright:** © 2023 by the authors. Licensee MDPI, Basel, Switzerland. This article is an open access article distributed under the terms and conditions of the Creative Commons Attribution (CC BY) license (<https://creativecommons.org/licenses/by/4.0/>).

## 1. Introduction

Mixed-anion compounds, such as oxynitrides, contain more than one anionic species in the structure. Such systems are of great interest since the introduction of two different anions in the structure adds new degrees of freedom to control the system and allows us to tune both the electronic and the atomic structures, thus achieving properties that are inaccessible to compounds containing only a single anion species. For example, oxynitrides can exhibit photocatalytic and magnetic properties [1–3] and can be used as dielectrics and non-toxic pigments [4,5]. Oxynitrides are expected to have smaller band gaps and better transport properties than the corresponding oxide. The band gap of oxide photocatalysts can be tuned by introducing nitrogen into the structure [6]. Furthermore, the oxides doped with nitrogen exhibit attractive elastic, catalytic, and optical properties and can be used as superionic conductors [7]. Usually, oxynitrides are more stable in air and moisture than pure nitrides [8].

In general, the structures of most mixed-anion compounds have been explored to a lesser degree than those of pure oxides or nitrides. Nevertheless, there are more than 7000 documents in the Scopus and WoS databases, which include oxynitride compounds, with a recent noticeable increase in the number of research papers; there are currently 612 oxynitride materials listed in the ICSD database according to Kageyama et al. [9]. Such mixed-anion systems have been the subject of recent studies [10–12], which mostly focus on property screening for known and hypothetical oxynitrides. In a recent work by Sharan et al. [13], a first-principles computational approach was used for the proposal of novel ternary oxide–nitride materials using the kinetically limited minimization (KLM) algorithm.

However, the preparation of nitrogen-doped oxides is not trivial. Considering the case of ceria, we find that inserting nonmetals in the  $\text{CeO}_2$  is uncommon, where successful doping significantly changes the physical and chemical properties of ceria [14–16]. Usually, ceria is doped with phosphorus, carbon, sulfur, europium, lanthanum, and praseodymium [17–20]. In this way, finding a stable ceramic compound with  $\text{Ce}_3\text{O}_3\text{N}$  composition would be attractive, both for science and technology, since this ceramic could have many intriguing properties.

Nevertheless, finding stable or metastable compounds with a Ce–O–N composition is not straightforward because cerium appears in its compounds with different oxidation numbers (+III) and (+IV), or even with both of the two valences. One of the most common compounds with Ce (+IV) is  $\text{CeO}_2$ , showing cubic symmetry ( $Fm-3m$ ) and fluorite structure type [21,22]. One more cerium oxide is  $\text{Ce}_2\text{O}_3$ , consisting of Ce in the (+III) oxidation state. Nevertheless,  $\text{Ce}_2\text{O}_3$  can exhibit both valences, which depend on the temperature, number of vacancies, foreign ions, and oxygen pressure [23,24].

Our idea was to investigate the cerium–oxygen–nitride compound. Since cerium appears in two oxidation states,  $\text{Ce}^{4+}$  in  $\text{Ce}_2\text{ON}_2$  and  $\text{Ce}^{3+}$  in  $\text{Ce}_3\text{O}_3\text{N}$ , it was necessary to investigate two completely different compositional subspaces of the Ce/O/N system. In our previous work, we identified possible modifications in  $\text{Ce}_2\text{ON}_2$ , combining structure prediction methods with local optimization [25]. We should emphasize the difference in global search settings for these two systems. Firstly, the ionic radius of  $\text{Ce}^{3+}$  is larger than  $\text{Ce}^{4+}$ , and this should be considered during a global search. Additionally,  $\text{Ce}^{4+}$  usually builds compounds with coordination VI, while  $\text{Ce}^{3+}$  prefers coordination VIII. Furthermore, the anion distribution is quite different since, in  $\text{Ce}_2\text{ON}_2$ , one formula unit consists of five atoms (three anions and two cations), while in  $\text{Ce}_3\text{O}_3\text{N}$ , one formula unit contains seven atoms (four anions and three cations).

In this study, we investigate the hypothetical cerium oxynitride  $\text{Ce}_3\text{O}_3\text{N}$  composition, with  $\text{Ce}^{3+}$  cations, utilizing computational methods; so far, only one proposed candidate structure exists, exhibiting monoclinic  $P2_1$  symmetry [13]. The candidates with different structures are generated using two approaches—the global optimization of the energy landscape and data mining search, followed by local optimization on the *ab initio* level of the most promising candidates. The two structure generation procedures find different sets of low-energy structures, which agrees with the general observation that employing a multi-method approach instead of using only a single tool to generate candidate structures is highly useful to efficiently increase the structural variety of the set of structure candidates.

## 2. Computational Details

Predicting feasible stable or metastable structures for the  $\text{Ce}_3\text{O}_3\text{N}$  system was performed using a two-step approach, integrating global optimization and data mining [26–28]. The global search (GS) of the energy landscape was performed in the first part of our study, and the results were supplemented by the outcome of a database search.

The enthalpy landscape of the  $\text{Ce}_3\text{O}_3\text{N}$  compound was explored for several pressures, utilizing simulated annealing [29] as an algorithm for the global search, combined with periodic local optimizations along the search trajectory. The standard stochastic simulated annealing based on (many) random Monte Carlo walks on the energy landscape was followed by periodic stochastic quenches, carried out with the G42+ code [30]. The global searches were accomplished for one, two, and three formula units and six different pressures in GPa (0; 0.016; 0.16; 1.6; 16, and 160). The move class of the random walk included the following moves: shifts in all atoms only (20%); random shift in atoms within a box around a randomly specified atom (30%); shift in all atoms and change in the cell parameters together with atom movement (20%); change in all cell parameters with fixed atoms (10%); and change in all cell parameters with atom movement (20%). This is usually combined with a short stochastic quench. To perform the global searches with a rational computational effort, a fast computable empirical two-body potential consisting of Lennard–Jones and Coulomb terms was employed [31].

Next, we performed data-mining-based explorations of the ICSD database, Refs. [32,33] to find additional structure candidates in the  $\text{Ce}_3\text{O}_3\text{N}$  system via analogy to known crystallographic structures. This data mining search gave us additional structure candidates since a global search is not reliable to identify every possible candidate. When globally searching on empirical energy landscapes, some important candidates may not be identified, either because of computation time limitations or because of the inherent limitations of the empirical potential as an energy function, i.e., these missing structures may not correspond to local minima on the empirical landscape. On the other hand, performing the complete global search on the *ab initio* landscape for complex systems is often not feasible due to the several orders of magnitude larger computational effort compared to the search on the empirical potential landscape. Therefore, data mining is a very useful supplementary method for identifying potential structure candidates in not-yet-synthesized chemical systems.

For the database mining, we employed a systematic procedure known as KDD (knowledge discovery in databases), involving selection, pre-processing, transformation, and interpretation/evaluation (or post-processing), to identify a sufficiently large number of structure candidates for the  $\text{Ce}_3\text{O}_3\text{N}$  system from the ICSD database [32,33]. In our first run, we found 76,415 candidates belonging to the ternary systems in the ICSD database. The results were filtered by introducing the general formula  $\text{AB}_3 \times 3$ , resulting in 298 structure candidates. The candidates with the formula  $\text{A}_3\text{B}_3\text{C}$  occurring in the ICSD were extracted, followed by a prototype analysis to reduce the excess of candidates to a feasible number of different types of structures [27,34,35]. After eliminating duplicates, we obtained 19 structure candidates (see Supplementary Information).

Finally, *ab initio* calculations of the total energy and *ab initio* local optimizations of the structure candidates found after global search and data mining were accomplished with the CRYSTAL17 code [36], ground on linear combinations of atomic orbitals. Analytical gradients were used for the local optimization runs [37,38]. Local optimizations were performed at the DFT level by applying the local density approximation (LDA). For the  $\text{Ce}^{3+}$ , a pseudopotential [39] was used with a [4s4p2d3f] basis set; for  $\text{O}^{2-}$ , a [4s3p] basis set was used [40,41], and for  $\text{N}^{3-}$  [3s2p], an all-electron basis set based on Gaussian-type orbitals was employed [42,43]. The symmetries of the analyzed structures were resolved using the program KPLOT [44]. Finally, structures were visualized using the Vesta software [45]. Here, we note that the local optimization of the data mining candidates often leads to quite substantial changes in the structure compared to the one originally extracted from the database, beyond just a simple rescaling of cell parameters.

### 3. Results and Discussion

#### 3.1. Candidates Generated via Global Exploration of the Energy Landscape at the Empirical Level

During the exploration of the enthalpy landscape using global optimization for different numbers of formula units ( $Z = 1, 2, 3$ ), and six different pressures (0, 0.016, 0.16, 1, 6, 16, and 160 GPa), we found over 10,000 structure candidates. Initially, for each of these structure candidates, the symmetry was determined using the KPLOT code and the algorithms SFND [46] and RGS [47] implemented therein. In this way, we sorted the initial structures according to the space groups. They were then compared with each other using the CMPZ algorithm [48] to find duplicates with the same structure types. To identify the best candidates for local optimization, the crystallographic features of the obtained structures were investigated in detail.

The global search results for various pressures and one formula unit of  $\text{Ce}_3\text{O}_3\text{N}$  are presented in Table 1. One can observe that most of the local minima correspond to strongly distorted structures with space group  $P1$ . In addition to these candidates, the enthalpy landscape of  $\text{Ce}_3\text{O}_3\text{N}$  with  $Z = 1$  contains many different structure candidates with non-trivial symmetry, i.e., a space group different from  $P1$  or  $P-1$ , for the 0 to 160 GPa pressure range. Most of the structure candidates show relatively low symmetry (triclinic and monoclinic), but some high-symmetry candidates appear. For  $Z = 1$ , apart from the  $P1$  structures, the most frequently observed structures appear in space groups  $Pm$  (no. 6)

and Cm (no. 8) (Table 1). Among the candidates with orthorhombic symmetry, the most common ones exhibit space groups *Pmm2* (no. 25) and *Amm2* (no. 38), while most of the structures with cubic symmetry appear in space group *Pm-3m* (no. 221).

**Table 1.** Frequency of the space groups obtained for the results of the search at a global level performed at different pressures for  $Z = 1$  of  $Ce_3O_3N$ .

Pressure (GPa)	Space Group No.																	
	1	3	5	6	8	10	16	25	38	44	47	99	115	146	155	160	207	221
0	379	-	-	32	11	-	-	7	-	2	-	1	-	-	-	-	-	-
0.016	376	2	1	27	7	-	-	10	2	-	-	1	1	-	1	-	1	3
0.16	368	-	-	38	3	1	1	5	-	1	1	1	-	-	-	-	3	10
1.6	373	1	2	26	9	-	-	7	3	-	-	1	-	-	1	-	2	7
16	370	2	3	25	10	-	-	-	7	2	-	-	-	-	-	-	6	7
160	332	-	3	36	20	1	1	5	16	1	11	-	-	4	-	2	-	-
$\Sigma$	2198	5	9	184	60	2	2	34	28	6	12	4	1	4	2	2	12	27

When the pressure increases, the number of distorted structures decreases. At the highest pressure in this study (160 GPa), only 332 structures with space group *P1* for  $Z = 1$  were obtained (Table 1).

For two formula units,  $Ce_6O_6N_2$ , the number of structure candidates found with non-trivial symmetry is much smaller than for  $Z = 1$ . Thus, the subsequent statistical and crystallographic analysis of the enthalpy landscapes with  $Z = 2$ , at pressures up to 160 GPa, yielded only a few additional candidates with non-trivial symmetry, all of which were discarded after the local optimization step as being unstable and/or of too high energy.

For  $Z = 3$ , there are no new structure candidates with non-trivial symmetry among the 4800 minimum configurations. Quite generally, we note that with an increase in the formula unit number, many more local minima with quite low energy corresponding to defect structures or that exhibit several different coordination polyhedra of Ce atoms by O and N atoms appear. Since these polyhedra are usually distorted due to the different ionic radii of  $O^{2-}$  and  $N^{3-}$ , and there are many ways to arrange the anions around the cation, the number of symmetries of such a structure is greatly reduced compared to the case of the minimal number of formula units/simulation cells. In particular, the anion arrangements in the coordination polyhedra often do not differ by much in energy, and, thus, they are also found during the global search. This is expected since when the composition of the chemical system exceeds two types of atoms, the number of local minima that correspond to structures containing “defects” increases (where “defect” here refers to the non-optimal distribution of the two types of anions over the corners of the coordination polyhedra around the Ce ions, which is slightly higher in energy than the optimal distribution), and, in this way, most of the structure candidates show *P1* (no. 1) symmetry, even though their energies are quite low.

Next, for each of the candidates with non-trivial symmetry from Table 1, a local optimization at the *ab initio* level was performed. After the local optimizations, we ranked the structures obtained according to the total energy values.

### 3.2. Candidates Generated via Data-Mining-Based Searches

The best structure candidates according to the total energy criterion are given in Table 2. The data mining search used the ICSD database [32], containing more than 200,000 inorganic structures. As a criterion for being chosen as structure candidates, we considered different structure prototypes in the ternary  $A_3B_3C$  system. After eliminating duplicate structures, we obtained 19 structure candidates:  $Al_3ScC_3$  [49],  $Ba_3FeN_3$  [50],  $Ca_3P_3$  [51],  $Ca_3InP_3$  [52],  $Cu_3SbS_3$  [53],  $Fe_3TlTe_3$  [54],  $Fe_3W_3C$  [55],  $Gd_3MnI_3$  [56],  $K_3AlSe_3$  [57],  $K_3BS_3$  [58],

$K_6Sn_2Te_6$  [59],  $KB_3H_3$  [60],  $Na_3AsS_3$  [61],  $Ni_3SmGe_3$  [62],  $NiSc_3Si_3$  [63], (proustite) [64],  $Rh_4C_{12}O_{12}$  [65],  $Tl_3AsSe_3$  [66], and  $Ag_3AsS_3$  (xanthoconite) [67].

**Table 2.** Energy ranking of the structure candidates from the global search (GS) and data mining (DM) after *ab initio* optimization. The total energy (in Eh) and relative energy values (in Eh and kcal/mol) per formula unit (f.u.) compared to the global minimum ( $Ce_3O_3N$ -DM1 structure taken as the zero of energy), computed using the LDA-PZ functional.

Modification	Space Group (No.)	Total Energy (Eh)	Relative Energy in Eh (kcal/mol)
$Ce_3O_3N$ -DM1	<i>R3c</i> (161)	−1702.4875	0
$Ce_3O_3N$ -GS1	<i>P2/m</i> (10)	−1702.4813	0.0062 (3.89)
$Ce_3O_3N$ -GS2	<i>Amm2</i> (38)	−1702.4685	0.0190 (11.92)
$Ce_3O_3N$ -GS3	<i>Imm2</i> (44)	−1702.4627	0.0248 (15.56)
$Ce_3O_3N$ -GS4	<i>Pmmm</i> (47)	−1702.4588	0.0287 (18.01)
$Ce_3O_3N$ -GS5	<i>Amm2</i> (38)	−1702.4576	0.0299 (18.76)
$Ce_3O_3N$ -GS6	<i>Pmmm</i> (47)	−1702.4509	0.0366 (22.97)
$Ce_3O_3N$ -GS7	<i>Pm-3m</i> (221)	−1702.4394	0.0481 (30.18)
$Ce_3O_3N$ -DM2	<i>P6<sub>3</sub>/m</i> (176)	−1702.4007	0.0868 (54.47)
$Ce_3O_3N$ -DM3	<i>I-43m</i> (217)	−1702.2837	0.2038 (127.89)

Following local optimization at the *ab initio* level using LDA, most of the data mining structure candidates became unfavorable according to the total energy compared to the candidate structures obtained via the global search. Only one candidate, obtained starting from  $Ag_3AsS_3$  (proustite) structure type after local optimization, yielded—after substantial rearrangements—the  $Ce_3O_3N$ -DM1 structure, which exhibited the lowest total energy among all structure candidates (Table 2). Among the structure candidates obtained during the global optimization, the one with the lowest total energy after the local optimization was  $Ce_3O_3N$ -GS1, adopting space group *P2/m* (no. 10), which is the same as the one found after the global search. Surprisingly, the  $Ce_3O_3N$ -GS1 structure candidate was not frequently observed during the global search on the empirical energy landscape (Table 1). Relative energies are also given in Table 2, showing the energy differences between the minima on the landscape. For further discussions, we considered all the structures with relative energies below 0.03 Eh/f.u. (corresponding to a temperature of ca. 1300 K) as the most favorable modification feasible for realistic experimental conditions.

In the next step, we computed the energy vs. volume curves (equations of state) at the *ab initio* level using the LDA functional for the six most relevant structure candidates in the  $Ce_3O_3N$  system (Figure 1). It appears that the  $Ce_3O_3N$ -DM1 modification is the global minimum with quite a dense structure, while all other local minima found after global search (GS1-GS5) appear in the low-density region with higher *ab initio* energies. As a consequence, the  $Ce_3O_3N$ -DM1 modification is expected to remain the thermodynamically preferred  $Ce_3O_3N$  phase at elevated pressures.

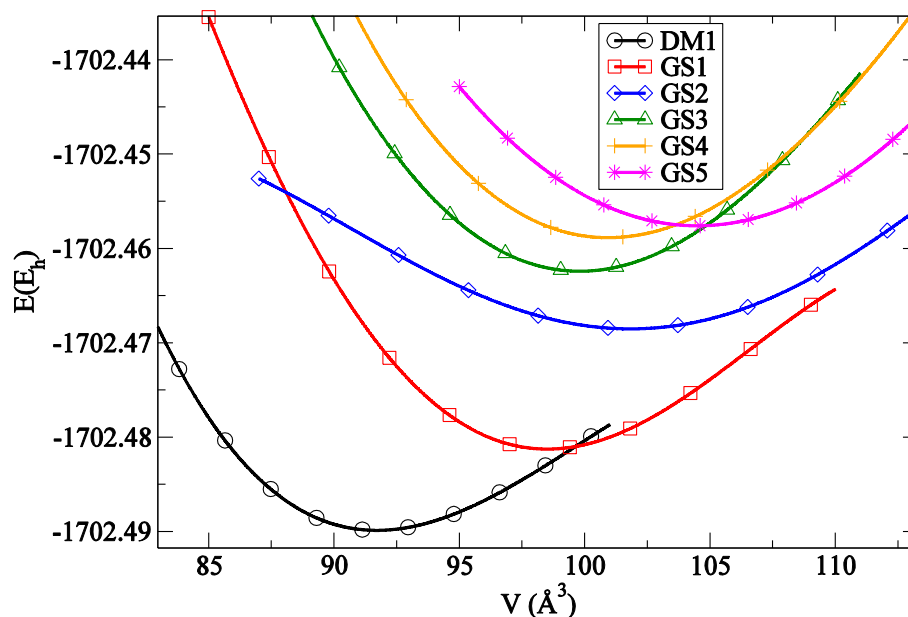


**Figure 1.** Energy vs. volume,  $E(V)$ , curves for the six most stable and energetically favorable structure candidates of  $\text{Ce}_3\text{O}_3\text{N}$  obtained using the LDA functional. Energies per formula unit are given in Hartree (Eh).

#### 4. Crystal Structure Analysis

Structure details, including unit cell parameters and atomic positions for the most relevant structure candidates, are given in Table 3. Bond lengths inside the different coordination polyhedra for the most relevant  $\text{Ce}_3\text{O}_3\text{N}$  modifications are presented in the Supplementary Material (Table S1). Furthermore, structure details for the structurally interesting but energetically not favorable structure candidates ( $\text{Ce}_3\text{O}_3\text{N}$ -GS6,  $\text{Ce}_3\text{O}_3\text{N}$ -GS7,  $\text{Ce}_3\text{O}_3\text{N}$ -DM2, and  $\text{Ce}_3\text{O}_3\text{N}$ -DM3) are also shown in Tables S1–S3 and Figure 5.

**Table 3.** Space group, unit cell parameters (Å), and atomic positions for the most relevant  $\text{Ce}_3\text{O}_3\text{N}$  modifications.

Modification	Space Group (No.)	Cell Parameters (Å) and Fractional Coordinates
$\text{Ce}_3\text{O}_3\text{N}$ -DM1	$R3c$ (161)	$a = 10.17; c = 6.15$ Ce (−0.1996 −0.0378 0.2416) O (−0.0656 0.2200 0.3762) N (0 0 0.0066)
$\text{Ce}_3\text{O}_3\text{N}$ -GS1	$P2/m$ (10)	$a = 5.89; b = 3.62; c = 5.04; \beta = 113.2^\circ$ Ce (0 0 0) Ce (0.3017 1/2 0.6238) O (0.2702 1/2 0.0652) O (1/2 0/2) N (0 0 1/2)
$\text{Ce}_3\text{O}_3\text{N}$ -GS2	$Amm2$ (38)	$a = 3.59; b = 9.83; c = 5.78$ Ce (1/2 0 0.1729 0.8911) Ce (0 0 0.3964) Ce (1/2 0 0.8038) O (0.5 0 0.1402) O (0 0.7712 0.1681) N (1/2 0 0.6528)

Table 3. Cont.

Modification	Space Group (No.)	Cell Parameters (Å) and Fractional Coordinates
Ce <sub>3</sub> O <sub>3</sub> N-GS3	<i>Imm2</i> (44)	$a = 3.38; b = 3.39; c = 17.39$ Ce (0 0 0.7735) Ce (0 0 0.4276) Ce (0 0 0.0814) O (0 0 0.5589) O (0 0 0.2961) O (0 1/2 0.1775) N (0 0 0.9277)
Ce <sub>3</sub> O <sub>3</sub> N-GS4	<i>Pmmm</i> (47)	$a = 6.86; b = 3.53; c = 4.62$ Ce (1/2 0 0) Ce (0.7607 1/2 1/2) O (0.2869 1/2 0) O (0 0 1/2) N (1/2 0 1/2)
Ce <sub>3</sub> O <sub>3</sub> N-GS5	<i>Amm2</i> (38)	$a = 3.49; b = 3.32; c = 17.93$ Ce (1/2 0 0.0970) Ce (0 0 0.4475) Ce (1/2 0 0.8038) O (0 0 0.5730) O (0 0 0.3143) O (1/2 0 0.6850) N (1/2 0 0.9444)

The Ce<sub>3</sub>O<sub>3</sub>N-DM1 modification exhibits the trigonal space group *R3c* (no. 161). Cerium is 8-fold coordinated with six oxygen and two nitrogen atoms, with a mean distance of about 2.48 Å. As remarked above, the structure of the Ce<sub>3</sub>O<sub>3</sub>N-DM1 (Figure 2a) modification noticeably differs from the initial Ag<sub>3</sub>As<sub>3</sub> (proustite) structure type shown in Figure 2b: starting from the initial proustite [64] structure type, the local optimization resulted in a completely different arrangement of atoms while keeping the space group *R3c* (161).

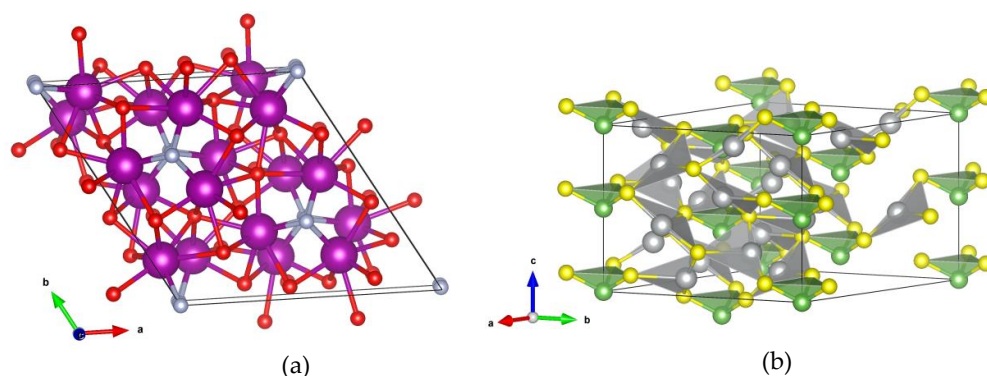


**Figure 2.** Visualization of structure for (a) Ce<sub>3</sub>O<sub>3</sub>N-DM1 modification in space group *R3c* (161); (b) initial Ag<sub>3</sub>As<sub>3</sub> (proustite) structure type. Cerium, oxygen, and nitrogen atoms are shown as violet, red, and grey spheres, respectively.

It is noteworthy that the Ce<sub>3</sub>O<sub>3</sub>N-DM1 modification was only found via an intermediary structure candidate using data mining, and that, in compliance with the E(V) curves, the Ce<sub>3</sub>O<sub>3</sub>N-DM1 modification is a distinctive equilibrium structure type and global minimum up to high pressures.

The Ce<sub>3</sub>O<sub>3</sub>N-GS1 structure candidate is in the space group *P2/m* (no. 10) and was found after the global optimization. The structure is shown in Figure 3a where the unit

cell parameters are:  $a = 5.89 \text{ \AA}$ ;  $b = 3.62 \text{ \AA}$ ;  $c = 5.04 \text{ \AA}$ , and  $\beta = 113.3^\circ$ . Cerium is in 7-fold coordination (with atom–atom distances of  $2 \times 2.37 \text{ \AA—O}$ ,  $2 \times 2.44 \text{ \AA—N}$ ,  $1 \times 2.30 \text{ \AA—O}$ ,  $1 \times 2.39 \text{ \AA—O}$ ,  $1 \times 2.75 \text{ \AA—O}$ ), where the mean distance is  $2.53 \text{ \AA}$ , and 6-fold coordination (with atom–atom distances of  $4 \times 2.34 \text{ \AA—O}$ ,  $2 \times 2.52 \text{ \AA—N}$ ), where the mean distance is  $2.40 \text{ \AA}$ . However, the one 6-fold coordinated cerium atom resides inside a nice octahedral polyhedron, while the other Ce atom is surrounded by a distorted octahedron since it has one longer bond to an oxygen atom ( $1 \times 2.75 \text{ \AA—O}$ ), and it might be regarded as a 6 + 1 coordination. This structure is the most stable candidate from the global search output and is ranked second in Figure 1. Inspecting the  $E(V)$  curves, one can expect this modification to be the preferred one in the effective negative pressure region where a phase transformation from  $\text{Ce}_3\text{O}_3\text{N-DM1}$  to  $\text{Ce}_3\text{O}_3\text{N-GS1}$  may occur. This could indicate a possible synthesis route via, e.g., crystallization from an amorphous phase deposited from the gas phase, as was recently used in the synthesis of a new gallium modification ( $\beta'$ -gallium) [68].

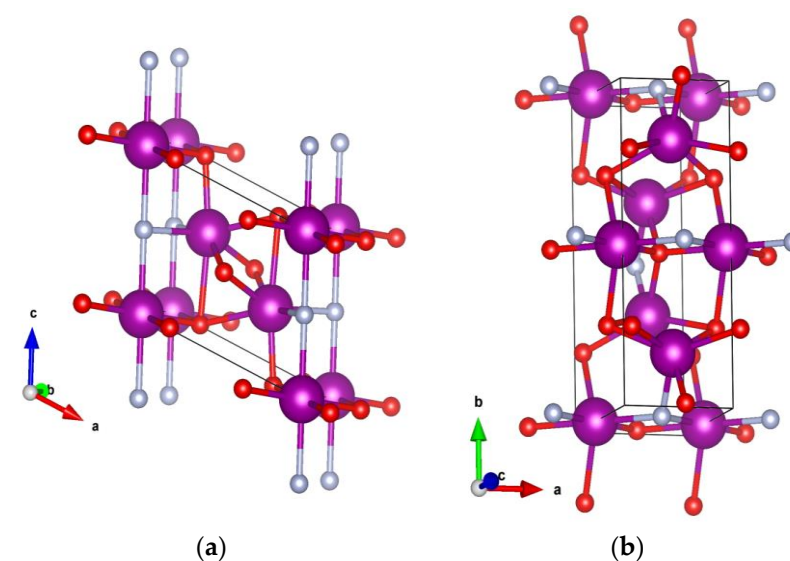


**Figure 3.** Visualization of the structure for (a)  $\text{Ce}_3\text{O}_3\text{N-GS1}$  in monoclinic space group  $P2/m$ ; (b)  $\text{Ce}_3\text{O}_3\text{N-GS2}$  in orthorhombic space group  $Amm2$ . Cerium, oxygen, and nitrogen atoms are shown as violet, red, and grey spheres, respectively.

Among the many candidates with orthorhombic symmetry, the  $\text{Ce}_3\text{O}_3\text{N-GS2}$  modification is the most stable one and is ranked as the third one in total energy (Figures 1 and 3b). This structure type is characterized by Ce atoms in distorted octahedral coordination. In the first type of octahedra, with a mean Ce-anion distance of  $2.36 \text{ \AA}$ , there is only one nitrogen atom, while in the second type of octahedra, with a mean distance of  $2.42 \text{ \AA}$ , two nitrogen atoms are present. Nevertheless, these polyhedra are strongly deformed where the distances from the Ce ions to the oxygen and nitrogen anions range from  $2.23$  to  $2.61 \text{ \AA}$  (Figure 3b).

There are four candidates with orthorhombic symmetry among the top five GS modifications according to the total energy ranking (Table 1). In addition to the above-mentioned  $\text{Ce}_3\text{O}_3\text{N-GS2}$  modification with orthorhombic  $Amm2$  (sg. 38) symmetry, there are  $\text{Ce}_3\text{O}_3\text{N-GS3}$ ,  $\text{Ce}_3\text{O}_3\text{N-GS4}$ , and  $\text{Ce}_3\text{O}_3\text{N-GS5}$  with  $Imm2$  (sg. 44),  $Pmmm$  (sg. 47),  $Amm2$  (sg. 38) space groups, respectively.

Next, the orthorhombic modifications (especially with sg. 38 and 44) were found to be favorable modifications at high pressures during global optimization with empirical potential (Table 1). After DFT local optimization, these structures appeared to belong to the high-temperature region as metastable phases, which would indicate the need for elevated pressures and temperatures during their synthesis.

In the  $\text{Ce}_3\text{O}_3\text{N-GS3}$  structure, there are two kinds of polyhedra, building two different alternating layers (Figure 4a). In the first layer, where oxygen prevails, there is a Ce cation

coordinated with six oxygen atoms and one nitrogen atom. Another layer is made from octahedra with four nitrogen atoms with the same bond length Ce–N of 2.39 Å, and two oxygen atoms at approximately the same distance of 2.28 Å. This structure is interesting since we, for the first time, have a candidate where the oxygen and nitrogen atoms tend to separate and arrange themselves in layers. This kind of arrangement is not as energetically favorable as those of structures DM1, GS1, and GS2, where the distribution of the anions is more random.

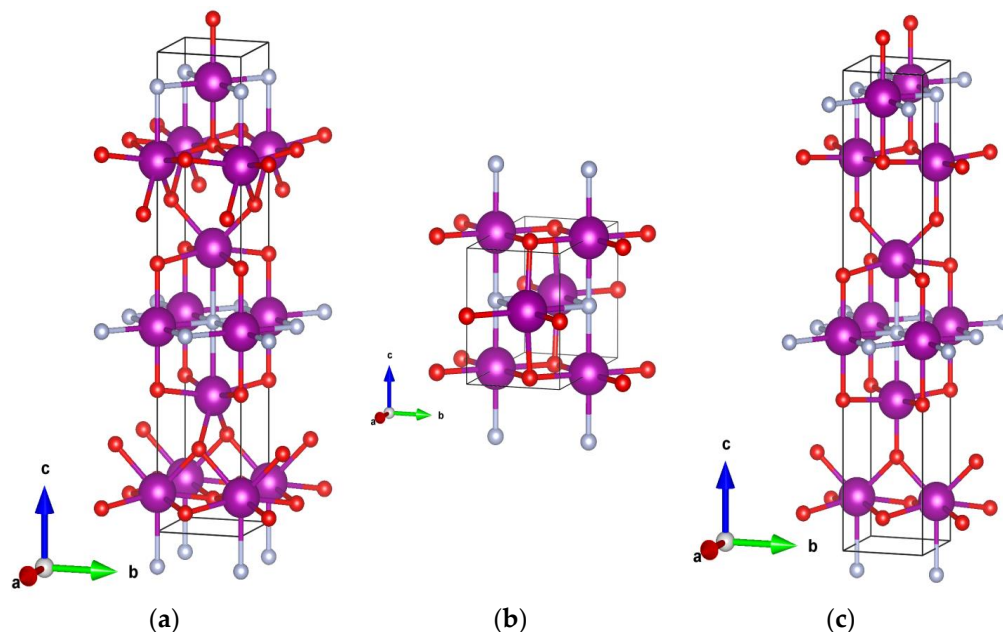


**Figure 4.** Visualization of structure for three orthonorhombic global search candidates: (a)  $\text{Ce}_3\text{O}_3\text{N}$ -GS3 in space group  $Imm2$ ; (b)  $\text{Ce}_3\text{O}_3\text{N}$ -GS4 in space group  $Pmmm$ ; and (c)  $\text{Ce}_3\text{O}_3\text{N}$ -GS5 in space group  $Amm2$ . Cerium, oxygen, and nitrogen atoms are shown as violet, red, and grey spheres, respectively.

Only the octahedral coordination of cerium is present in the  $\text{Ce}_3\text{O}_3\text{N}$ -GS4 structure candidate (Figure 4b), in contrast to the  $\text{Ce}_3\text{O}_3\text{N}$ -GS1 and  $\text{Ce}_3\text{O}_3\text{N}$ -GS3 structures where we also had a seven-fold coordination of cerium. One should emphasize the difference in the mean Ce-anion distances of the octahedra: there are octahedra with a mean Ce-anion distance of 2.30 Å, and another one with an average Ce-anion distance of 2.42 Å. Interestingly, both octahedra include four oxygen and two nitrogen atoms.

The last promising GS modification considered in the energy vs. volume,  $E(V)$ , curves (Figure 1) for  $\text{Ce}_3\text{O}_3\text{N}$ -GS5, as shown in Figure 4c. We note that  $\text{Ce}_3\text{O}_3\text{N}$ -GS3 and  $\text{Ce}_3\text{O}_3\text{N}$ -GS5 are related: they are close in energy, both designate high-pressure and high-temperature synthesis conditions, and both appear in orthonorhombic symmetry (Figure 3a,c). Furthermore, they have similar structures, with the same coordination polyhedra (6- and 7-fold). The main difference is in the way the polyhedra are connected. They appear as polytypes, similar to what we found in our previous studies [69–71]. The separation of layers where oxygen dominates from the layers with mostly nitrogen anions is pronounced.

There is one more GS candidate that should be mentioned, even if it is energetically not as favorable as the modifications included in Figure 1. This structure is mentioned in Table 1 as  $\text{Ce}_3\text{O}_3\text{N}$ -GS7 with  $Pm-3m$  (221) symmetry and shown in Figure 5b. Interestingly, local optimizations of various configurations initially exhibiting space groups  $R3$  (sg. 146),  $R3m$  (sg. 160),  $P4mm$  (sg. 99),  $P432$  (sg. 207), and  $R32$  (sg. 155) all resulted in the conversion of the starting structures into a modification with cubic  $Pm-3m$  (sg. 221) symmetry. This suggests that this candidate represents a large local multi-minimum basin at an empirical potential level. Additionally, since structures with space groups 160 and 99 are only found in the high-pressure regime (160 Gpa) during the global search (Table 2), structures with

this cubic  $Pm-3m$  (221) symmetry can be expected to be of relevance at extremely high pressures in the  $Ce_3O_3N$  system.

Regarding other structures we obtained after the local DFT optimization, starting from either the global search minima or the data mining results, we will not discuss them in detail since we consider them energetically unfavorable. Figure 5 shows the visualization of predicted non-favorable structures of  $Ce_3O_3N$ : the  $Ce_3O_3N$ -GS6 in the orthorhombic space group  $Pmmm$  (Figure 5a); the  $Ce_3O_3N$ -GS7 in the cubic space group  $Pm-3m$  (Figure 5b); the  $Ce_3O_3N$ -DM2 in the hexagonal space group  $P6_3/m$  (Figure 5c); and  $Ce_3O_3N$ -DM3 in the cubic space group  $I-43m$  (Figure 5d). Tables with their full structural details are given in the Supplementary Material (Tables S2 and S3). Specifically, the data mining candidates, except the  $Ce_3O_3N$ -DM1 modification, are very high in total energy (Table 1) and are, thus, not of interest for further analysis.

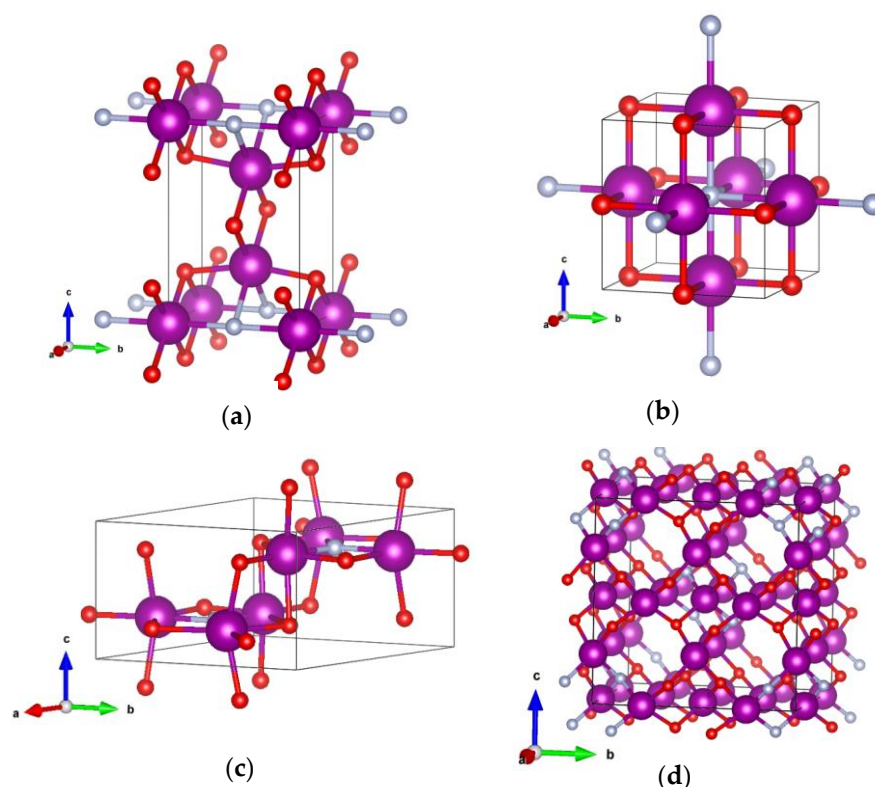


**Figure 5.** Visualization of the structure for (a)  $Ce_3O_3N$ -GS6 in space group  $Pmmm$ ; (b)  $Ce_3O_3N$ -GS7 in space group  $Pm-3m$ ; (c)  $Ce_3O_3N$ -DM2 in space group  $P6_3/m$ ; and (d)  $Ce_3O_3N$ -DM3 in space group  $I-43m$ . Cerium, oxygen, and nitrogen atoms are shown as violet, red, and grey spheres, respectively.

Finally, it is interesting to record that in the five relevant GS structure candidates, the cerium cations are seven- or six-fold coordinated by the anions, where the only difference is the coordination polyhedra shape and the connection between them. On the other hand, the energetically most favorable modification,  $Ce_3O_3N$ -DM1, comprises eight-fold coordinated polyhedra around Ce cations. This suggests that the ratio of the ionic radii between  $Ce^{3+}$  and  $O^{2-}$  and  $N^{3-}$  might be too small in the parameters of the empirical potential employed, which had been fitted originally to the binary  $Ce_2O_3$  and  $CeN$  structures. Furthermore, it demonstrates the general observation that not a single exploration method but a combination of several, such as global search and data mining for the  $Ce_3O_3N$  system studied here, is most effective for finding sets of suitable candidates of a not-yet-synthesized chemical compound [72].

In the literature, there was a recent proposal of a structure candidate for the  $Ce_3O_3N$  system in the space group  $P2_1$  (no. 4) [13]. We optimized the proposed structure candidate together with the best candidates from the global and data mining search ( $Ce_3O_3N$ -DM1

and  $\text{Ce}_3\text{O}_3\text{N-GS1}$ ) using the VASP code and the LDA functional for comparison, since the optimization in the literature structure was not possible with the CRYSTAL17 code. According to the VASP calculations, the proposed structure candidate from the literature has a higher energy than the present  $\text{Ce}_3\text{O}_3\text{N-DM1}$  and  $\text{Ce}_3\text{O}_3\text{N-GS1}$  candidates (see Supplementary Information, Table S4). Of course, there is a possibility for changes in the total energy ranking by using a different functional (e.g., GGA), basis set, etc., and, thus, the corresponding predicted structure in the space group  $P2_1$  (no. 4) [13] should be included as a potential structure candidate for experimental synthesis in the Ce/O/N system with Ce in the oxidation stage III.

While this study focuses on the single ternary system  $\text{Ce}_3\text{O}_3\text{N}$  and the determination of possible candidate modifications of this composition, it is interesting to know whether these candidates would be thermodynamically stable or metastable with regard to the decomposition into the boundary phases  $\text{Ce}_2\text{O}_3$  and  $\text{CeN}$ ,  $\text{Ce}_3\text{O}_3\text{N} \Rightarrow \text{Ce}_2\text{O}_3 + \text{CeN}$ . After computing the *ab initio* energies of  $\text{Ce}_2\text{O}_3$  and  $\text{CeN}$  at the same level of accuracy as for  $\text{Ce}_3\text{O}_3\text{N}$ , we found that the total energy of  $\text{Ce}_3\text{O}_3\text{N-DM1}$  was higher than the sum of total energies for  $\text{Ce}_2\text{O}_3 + \text{CeN}$ . The difference is 0.62 eV per formula unit, i.e., about 0.09 eV/atom, which indicates that, at low temperatures,  $\text{Ce}_3\text{O}_3\text{N-DM1}$  would be thermodynamically unstable against such a decomposition. Nevertheless, this does not mean that this mixed cerium oxynitride compound could not be kinetically stable at low temperatures, i.e., once such a modification has been synthesized, it might well be stable for long periods at sufficiently low temperatures and, thus, could be employed in applications.

## 5. Conclusions

In this study, we explored the energy landscape of the not-yet-synthesized cerium oxynitride  $\text{Ce}_3\text{O}_3\text{N}$  ceramic and predicted several feasible modifications for this compound. The prediction of new modifications with the composition  $\text{Ce}_3\text{O}_3\text{N}$  was performed by combining global optimization at the empirical potential level with a data mining procedure, where the energy landscape was explored for different pressure values and various numbers of formula units in the simulation cell. In the second step, local structure optimizations of the candidates obtained during the global search and the data mining prototyping approach were performed at the *ab initio* level, and the structures of the various candidates were analyzed. This analysis showed that by combining global search and data mining, we obtained six low-energy modifications that could be realized as (meta)stable modifications, thus emphasizing the importance of combining different methods in the search for feasible structure candidates, especially in hypothetical systems.

For the fixed composition  $\text{Ce}_3\text{O}_3\text{N}$ , i.e., without considering a possible decomposition into the boundary phases  $\text{Ce}_2\text{O}_3$  and  $\text{CeN}$ , the  $\text{Ce}_3\text{O}_3\text{N-DM1}$  modification, with an  $\text{Ag}_3\text{AsS}_3$  (proustite) structure, is predicted to be the thermodynamically stable modification in standard conditions. The stability of  $\text{Ce}_3\text{O}_3\text{N-DM1}$  also extends to high pressures, while at effective negative pressures, the  $\text{Ce}_3\text{O}_3\text{N-GS1}$  modification should be synthetically accessible. Four predicted orthorhombic modifications,  $\text{Ce}_3\text{O}_3\text{N-DM2}$ , 3, 4, and 5, might be stable at high temperatures. Following on from our earlier study of the feasible modifications of composition  $\text{Ce}_2\text{ON}_2$  [25], this work provides a further glimpse into the potential structural richness of the Ce-O-N system and supports attempts to synthesize the predicted modifications of  $\text{Ce}_3\text{O}_3\text{N}$ , guided by our analysis of the energy landscape of this chemical system.

**Supplementary Materials:** The following supporting information can be downloaded at: <https://www.mdpi.com/article/10.3390/cryst13050774/s1>. Table S1: Bond lengths inside of different coordination polyhedra for various  $\text{Ce}_3\text{O}_3\text{N}$  modifications; Table S2: Space group, unit cell parameters (Å), atomic positions, and total energy values in Hartrees (Eh) for eight optimized modifications found using the global search method; Table S3: Space group, unit cell parameters (Å), atomic positions, and total energy values in Hartrees (Eh) for three optimized modifications found using the data mining method; Table S4: Total energy ranking in eV for the best candidates from the global

energy landscape and data-mining searches ( $\text{Ce}_3\text{O}_3\text{N-DM1}$ , and  $\text{Ce}_3\text{O}_3\text{N-GS1}$ ) and literature data calculated using the VASP code and the LDA functional.

**Author Contributions:** D.Z., B.M. and J.C.S. conceived the idea; the global search and *ab initio* structure optimizations were performed by D.Z. and J.Z.; M.P.Đ. collected and analyzed the literature and computational data, M.P. collected and analyzed the literature and computational data. All authors contributed to the discussion and writing of the paper. All authors have read and agreed to the published version of the manuscript.

**Funding:** This research was funded by the Ministry of Science, Technological Development and Innovation of the Republic of Serbia through Contract No. 451-03-47/2023-01/200017.

**Data Availability Statement:** Not applicable.

**Acknowledgments:** The authors are grateful to R. Dovesi, K. Doll, and Crystal Solutions for software support with CRYSTAL code.

**Conflicts of Interest:** The authors declare no conflict of interest.

## References

1. Higashi, M.; Abe, R.; Takata, T.; Domen, K. Photocatalytic Overall Water Splitting under Visible Light Using  $\text{ATaO}_2\text{N}$  (A = Ca, Sr, Ba) and  $\text{WO}_3$  in a  $\text{IO}_3^-/\text{I}^-$  Shuttle Redox Mediated System. *Chem. Mater.* **2009**, *21*, 1543–1549. [[CrossRef](#)]
2. Yang, M.; Oró-Solé, J.; Kusmartseva, A.; Fuertes, A.; Attfield, J.P. Electronic Tuning of Two Metals and Colossal Magnetoresistances in  $\text{EuWO}_{1+x}\text{N}_{2-x}$  Perovskites. *J. Am. Chem. Soc.* **2010**, *132*, 4822–4829. [[CrossRef](#)] [[PubMed](#)]
3. Jorge, A.B.; Oró-Solé, J.; Bea, A.M.; Mufti, N.; Palstra, T.T.M.; Rodgers, J.A.; Attfield, J.P.; Fuertes, A. Large Coupled Magnetoresponses in  $\text{EuNbO}_2\text{N}$ . *J. Am. Chem. Soc.* **2008**, *130*, 12572–12573. [[CrossRef](#)]
4. Kim, Y.-I.; Woodward, P.M.; Baba-Kishi, K.Z.; Tai, C.W. Characterization of the Structural, Optical, and Dielectric Properties of Oxynitride Perovskites  $\text{AMO}_2\text{N}$  (A = Ba, Sr, Ca; M = Ta, Nb). *Chem. Mater.* **2004**, *16*, 1267–1276. [[CrossRef](#)]
5. Jansen, M.; Letschert, H.P. Inorganic yellow-red pigments without toxic metals. *Nature* **2000**, *404*, 980–982. [[CrossRef](#)] [[PubMed](#)]
6. Jorge, A.B.; Fraxedas, J.; Cantarero, A.; Williams, A.J.; Rodgers, J.; Attfield, J.P.; Fuertes, A. Nitrogen Doping of Ceria. *Chem. Mater.* **2008**, *20*, 1682–1684. [[CrossRef](#)]
7. Lee, J.-S.; Lerch, M.; Maier, J. Nitrogen-doped zirconia: A comparison with cation stabilized zirconia. *J. Solid State Chem.* **2006**, *179*, 270–277. [[CrossRef](#)]
8. Sun, Y.; Lin, S.; Li, W.; Cheng, S.; Zhang, Y.; Liu, Y.; Liu, W. Review on Alkali Element Doping in  $\text{Cu}(\text{In,Ga})\text{Se}_2$  Thin Films and Solar Cells. *Engineering* **2017**, *3*, 452–459.
9. Kageyama, H.; Hayashi, K.; Maeda, K.; Attfield, J.P.; Hiroi, Z.; Rondinelli, J.M.; Poeppelmeier, K.R. Expanding frontiers in materials chemistry and physics with multiple anions. *Nat. Commun.* **2018**, *9*, 772. [[CrossRef](#)]
10. Wu, Y.; Lazic, P.; Hautier, G.; Persson, K.; Ceder, G. First principles high throughput screening of oxynitrides for water-splitting photocatalysts. *Energy Environ. Sci.* **2013**, *6*, 157–168. [[CrossRef](#)]
11. Sawada, K.; Nakajima, T. High-throughput screening of perovskite oxynitride and oxide materials for visible-light photocatalysis. *APL Mater.* **2018**, *6*, 101103.
12. Castelli, I.E.; Olsen, T.; Datta, S.; Landis, D.D.; Dahl, S.; Thygesen, K.S.; Jacobsen, K.W. Computational screening of perovskite metal oxides for optimal solar light capture. *Energy Environ. Sci.* **2012**, *5*, 5814–5819.
13. Sharan, A.; Lany, S. Computational discovery of stable and metastable ternary oxynitrides. *J. Chem. Phys.* **2021**, *154*, 234706. [[CrossRef](#)]
14. Prabhakaran, V.; Ramani, V. Structurally-Tuned Nitrogen-Doped Cerium Oxide Exhibits Exceptional Regenerative Free Radical Scavenging Activity in Polymer Electrolytes. *J. Electrochem. Soc.* **2013**, *161*, F1–F9.
15. Zhang, Y.C.; Liu, Y.K.; Zhang, L.; Xiu-tian-feng, E.; Pan, L.; Zhang, X.; Zou, D.R.; Liu, S.H.; Zou, J.J. DFT study on water oxidation on nitrogen-doped ceria oxide. *Appl. Surf. Sci.* **2018**, *452*, 423–428.
16. Mao, C.; Zhao, Y.; Qiu, X.; Zhu, J.; Burda, C. Synthesis, characterization and computational study of nitrogen-doped  $\text{CeO}_2$  nanoparticles with visible-light activity. *Phys. Chem. Chem. Phys.* **2008**, *10*, 5633–5638. [[CrossRef](#)]
17. Shi, H.; Hussain, T.; Ahuja, R.; Kang, T.W.; Luo, W. Role of vacancies, light elements and rare-earth metals doping in  $\text{CeO}_2$ . *Sci. Rep.* **2016**, *6*, 31345.
18. Matović, B.; Dukić, J.; Babić, B.; Bučevac, D.; Dohčević-Mitrović, Z.; Radović, M.; Bošković, S. Synthesis, calcination and characterization of Nanosized ceria powders by self-propagating room temperature method. *Ceram. Int.* **2013**, *39*, 5007–5012. [[CrossRef](#)]
19. Dmitrović, S.; Nikolić, M.G.; Jelenković, B.; Prekajski, M.; Rabasović, M.; Zarubica, A.; Branković, G.; Matović, B. Photoluminescent properties of spider silk coated with Eu-doped nanoceria. *J. Nanoparticle Res.* **2017**, *19*, 1–11.
20. Mićović, D.; Pagnacco, M.C.; Banković, P.; Maletaškić, J.; Matović, B.; Djokić, V.R.; Stojmenović, M. The influence of short thermal treatment on structure, morphology and optical properties of Er and Pr doped ceria pigments: Comparative study. *Process. Appl. Ceram.* **2019**, *13*, 310–321. [[CrossRef](#)]

21. Wołczyrz, M.; Kepinski, L. Rietveld refinement of the structure of CeOCl formed in Pd/CeO<sub>2</sub> catalyst: Notes on the existence of a stabilized tetragonal phase of La<sub>2</sub>O<sub>3</sub> in La-Pd-O system. *J. Solid State Chem. Fr.* **1992**, *99*, 409–413. [[CrossRef](#)]
22. Coduri, M.; Scavini, M.; Allietta, M.; Brunelli, M.; Ferrero, C. Defect Structure of Y-Doped Ceria on Different Length Scales. *Chem. Mater.* **2013**, *25*, 4278–4289. [[CrossRef](#)]
23. Mamontov, E.; Egami, T.; Brezny, R.; Koranne, M.; Tyagi, S. Lattice Defects and Oxygen Storage Capacity of Nanocrystalline Ceria and Ceria-Zirconia. *J. Phys. Chem. B* **2000**, *104*, 11110–11116. [[CrossRef](#)]
24. Skorodumova, N.V.; Ahuja, R.; Simak, S.I.; Abrikosov, I.A.; Johansson, B.; Lundqvist, B.I. Electronic, bonding, and optical properties of CeO<sub>2</sub> and Ce<sub>2</sub>O<sub>3</sub> from first principles. *Phys. Rev. B* **2001**, *64*, 115108. [[CrossRef](#)]
25. Zagorac, J.; Schön, J.C.; Matović, B.; Škundrić, T.; Zagorac, D. Predicting Feasible Modifications of Ce<sub>2</sub>ON<sub>2</sub> Using a Combination of Global Optimization and Data Mining. *J. Phase Equilibria Diffus.* **2020**, *41*, 538–549. [[CrossRef](#)]
26. Čebela, M.; Zagorac, D.; Batalović, K.; Radaković, J.; Stojadinović, B.; Spasojević, V.; Hercigonja, R. BiFeO<sub>3</sub> perovskites: A multidisciplinary approach to multiferroics. *Ceram. Int.* **2017**, *43*, 1256–1264. [[CrossRef](#)]
27. Zagorac, J.; Zagorac, D.; Rosić, M.; Schön, J.C.; Matović, B. Structure prediction of aluminum nitride combining data mining and quantum mechanics. *CrystEngComm* **2017**, *19*, 5259–5268. [[CrossRef](#)]
28. Zagorac, D.; Schön, J.C.; Rosić, M.; Zagorac, J.; Jordanov, D.; Luković, J.; Matović, B. Theoretical and Experimental Study of Structural Phases in CoMoO<sub>4</sub>. *Cryst. Res. Technol.* **2017**, *52*, 1700069. [[CrossRef](#)]
29. Kirkpatrick, S.; Gelatt, C.D.; Vecchi, M.P. Optimization by Simulated Annealing. *Science* **1983**, *220*, 671–680. [[CrossRef](#)]
30. Schön, J.C. Nanomaterials—What energy landscapes can tell us. *Process. Appl. Ceram.* **2015**, *9*, 157–168. [[CrossRef](#)]
31. Schön, J.C.; Jansen, M. Determination of candidate structures for simple ionic compounds through cell optimisation. *Comput. Mater. Sci.* **1995**, *4*, 43–58. [[CrossRef](#)]
32. Bergerhoff, G.; Brown, I.D. *Crystallographic Databases*; International Union of Crystallography: Chester, UK, 1987.
33. Zagorac, D.; Muller, H.; Ruehl, S.; Zagorac, J.; Rehme, S. Recent developments in the Inorganic Crystal Structure Database: Theoretical crystal structure data and related features. *J. Appl. Crystallogr.* **2019**, *52*, 918–925. [[CrossRef](#)] [[PubMed](#)]
34. Sokol, A.A.; Catlow, C.R.A.; Miskufova, M.; Shevlin, S.A.; Al-Sunaidi, A.A.; Walsh, A.; Woodley, S.M. On the problem of cluster structure diversity and the value of data mining. *Phys. Chem. Chem. Phys.* **2010**, *12*, 8438–8445. [[CrossRef](#)] [[PubMed](#)]
35. Ceder, G.; Morgan, D.; Fischer, C.; Tibbetts, K.; Curtarolo, S. Data-Mining-Driven Quantum Mechanics for the Prediction of Structure. *MRS Bull.* **2011**, *31*, 981–985. [[CrossRef](#)]
36. Dovesi, R.; Orlando, R.; Civalieri, B.; Roetti, C.; Saunders Victor, R.; Zicovich-Wilson Claudio, M. CRYSTAL: A computational tool for the *ab initio* study of the electronic properties of crystals. *Z. Für Krist. Cryst. Mater.* **2005**, *220*, 571. [[CrossRef](#)]
37. Doll, K.; Dovesi, R.; Orlando, R. Analytical Hartree–Fock gradients with respect to the cell parameter for systems periodic in three dimensions. *Theor. Chem. Acc.* **2004**, *112*, 394–402. [[CrossRef](#)]
38. Doll, K.; Saunders, V.R.; Harrison, N.M. Analytical Hartree–Fock gradients for periodic systems. *Int. J. Quantum Chem.* **2001**, *82*, 1–13. [[CrossRef](#)]
39. Graciani, J.; Márquez, A.M.; Plata, J.J.; Ortega, Y.; Hernández, N.C.; Meyer, A.; Zicovich-Wilson, C.M.; Sanz, J.F. Comparative Study on the Performance of Hybrid DFT Functionals in Highly Correlated Oxides: The Case of CeO<sub>2</sub> and Ce<sub>2</sub>O<sub>3</sub>. *J. Chem. Theory Comput.* **2011**, *7*, 56–65. [[CrossRef](#)] [[PubMed](#)]
40. Towler, M.D.; Allan, N.L.; Harrison, N.M.; Saunders, V.R.; Mackrodt, W.C.; Aprà, E. *Ab initio* study of MnO and NiO. *Phys. Rev. B* **1994**, *50*, 5041–5054. [[CrossRef](#)]
41. Zagorac, D.; Schön, J.C.; Zagorac, J.; Jansen, M. Prediction of structure candidates for zinc oxide as a function of pressure and investigation of their electronic properties. *Phys. Rev. B* **2014**, *89*, 075201. [[CrossRef](#)]
42. Dovesi, R.; Causa', M.; Orlando, R.; Roetti, C.; Saunders, V.R. *Ab initio* approach to molecular crystals: A periodic Hartree–Fock study of crystalline urea. *J. Chem. Phys.* **1990**, *92*, 7402–7411. [[CrossRef](#)]
43. Zagorac, D.; Zagorac, J.; Djukic, M.B.; Jordanov, D.; Matović, B. Theoretical study of AlN mechanical behaviour under high pressure regime. *Theor. Appl. Fract. Mech.* **2019**, *103*, 102289. [[CrossRef](#)]
44. Hundt, R. *KPLOT, A Program for Plotting and Analyzing Crystal Structures*; Technicum Scientific Publishing: Stuttgart, Germany, 2016.
45. Momma, K.; Izumi, F. VESTA: A three-dimensional visualization system for electronic and structural analysis. *J. Appl. Crystallogr.* **2008**, *41*, 653–658. [[CrossRef](#)]
46. Hundt, R.; Schön, J.C.; Hannemann, A.; Jansen, M. Determination of symmetries and idealized cell parameters for simulated structures. *J. Appl. Crystallogr.* **1999**, *32*, 413–416. [[CrossRef](#)]
47. Hannemann, A.; Hundt, R.; Schön, J.C.; Jansen, M. A New Algorithm for Space-Group Determination. *J. Appl. Crystallogr.* **1998**, *31*, 922–928. [[CrossRef](#)]
48. Hundt, R.; Schön, J.C.; Jansen, M. CMPZ—An algorithm for the efficient comparison of periodic structures. *J. Appl. Crystallogr.* **2006**, *39*, 6–16. [[CrossRef](#)]
49. Tsokol, A.O.; Bodak, O.I.; Marusin, E.P.; Baivelman, M.G. Crystal structure of the compound ScAl<sub>3</sub>C<sub>3</sub>. *Sov. Phys. Crystallogr.* (=Kristallogr.) **1986**, *31*, 467–468.
50. Rabenau, A.; Kniep, R.; Höhn, P. Ba<sub>3</sub>[FeN<sub>3</sub>]: Ein neues Nitridoferrat(III) mit [CO<sub>3</sub>]<sup>2-</sup>-isosteren Anionen [FeN<sub>3</sub>]<sup>6-</sup>. *Z. Für Krist.* **1991**, *196*, 153–158. [[CrossRef](#)]

51. Lang, J.; Hamon, C.; Marchand, R.; Laurent, Y. Étude d'halogénopnictures. III. Structure de  $\text{Ca}_2\text{PI}$  et  $\text{Ca}_3\text{PI}_3$ . Surstructures de type NaCl. *Bull. De Minéralogie* **1974**, *97*, 6–12.
52. Cordier, G.; Schaefer, H.; Stelter, M. Neue Zintlphasen:  $\text{Ba}_3\text{GaSb}_3$ ,  $\text{Ca}_3\text{GaAs}_3$  und  $\text{Ca}_3\text{InP}_3$ . *Z. Fuer Nat. Teil B Anorg. Chem. Org. Chem.* **1985**, *40*, 1100–1104.
53. Machatsehki, F. XII. Präzisionsmessungen der Gitterkonstanten verschiedener Fehlerze. *Form. Und Struktur Derselben* **1928**, *68*, 204–222. [[CrossRef](#)]
54. Klepp, K.; Boller, H. Die Kristallstruktur von  $\text{TlFe}_3\text{Te}_3$ . *Mon. Für Chem. Chem. Mon.* **1979**, *110*, 677–684. [[CrossRef](#)]
55. Pollock, C.B.; Stadelmaier, H.H. The eta carbides in the Fe–W–C and Co–W–C systems. *Metall. Trans.* **1970**, *1*, 767–770. [[CrossRef](#)]
56. Ebihara, M.; Martin, J.D.; Corbett, J.D. Novel Chain and Oligomeric Condensed Cluster Phases for Gadolinium Iodides with Manganese Interstitials. *Inorg. Chem.* **1994**, *33*, 2079–2084. [[CrossRef](#)]
57. Crystal structure of hexapotassium di- $\mu$ -selenido-bis(diselenidoaluminate),  $\text{K}_6\text{Al}_2\text{Se}_6$ . *Z. Für Krist.* **1991**, *197*, 173–174. [[CrossRef](#)]
58. Kuchinke, J.; Jansen, C.; Lindemann, A.; Krebs, B. Syntheses and Crystal Structures of the Novel Ternary Thioborates  $\text{Na}_3\text{BS}_3$ ,  $\text{K}_3\text{BS}_3$ , and  $\text{Rb}_3\text{BS}_3$ . *Z. Anorg. Allg. Chem.* **2001**, *627*, 896–902. [[CrossRef](#)]
59. Dittmar, G. Die Kristallstrukturen von  $\text{K}_6[\text{Ge}_2\text{Te}_6]$  und  $\text{K}_6[\text{Sn}_2\text{Te}_6]$  und ihre kristall-chemische Beziehung zum  $\text{K}_6[\text{Si}_2\text{Te}_6]$ -Typ. *Z. Anorg. Allg. Chem.* **1979**, *453*, 68–78. [[CrossRef](#)]
60. Kuznetsov, I.Y.; Vinitskii, D.M.; Solntsev, K.A.; Kuznetsov, N.T.; Butman, L.A. The crystal structure of  $\text{K}_2\text{B}_6\text{H}_6$  and  $\text{Cs}_2\text{B}_6\text{H}_6$ . *Zhurnal Neorgnicheskoi Khimii* **1987**, *32*, 3112–3114.
61. Palazzi, M. Structure cristalline de l'orthotrithioarsenite trisodique  $\text{Na}_3\text{AsS}_3$ . *Acta Crystallogr. Sect. B* **1976**, *32*, 3175–3177. [[CrossRef](#)]
62. Mruz, O.Y.; Pecharskii, V.K.; Sobolev, A.N.; Bodak, O.I. Crystal structure of  $\text{SmNi}_3\text{Ge}_3$ . *Kristallografiya* **1990**, *35*, 202–204.
63. Kotur, B.Y.; Gladyshevskii, E.I. Crystal structure of scandium-nickel silicide ( $\text{Sc}_3\text{NiSi}_3$ ). *Kristallografiya* **1983**, *28*, 461–464.
64. Harker, D. The Application of the Three-Dimensional Patterson Method and the Crystal Structures of Proustite,  $\text{Ag}_3\text{AsS}_3$ , and Pyrargyrite,  $\text{Ag}_3\text{SbS}_3$ . *J. Chem. Phys.* **1936**, *4*, 381–390. [[CrossRef](#)]
65. Wei, C.H. Structural analyses of tetracobalt dodecacarbonyl and tetra-rhodium dodecacarbonyl. Crystallographic treatments of a disordered structure and a twinned composite. *Inorg. Chem.* **1969**, *8*, 2384–2397. [[CrossRef](#)]
66. Hong, H.Y.P.; Mikkelsen, J.C.; Roland, G.W. Crystal structure of  $\text{Tl}_3\text{AsSe}_3$ . *Mater. Res. Bull.* **1974**, *9*, 365–369. [[CrossRef](#)]
67. Engel, P.; Nowacki, W. Die Kristallstruktur von Xanthokon,  $\text{Ag}_3\text{AsS}_3$ . *Acta Crystallogr. Sect. B* **1968**, *24*, 77–81. [[CrossRef](#)]
68. Fischer, D.; Andriyevsky, B.; Schön, C. Systematics of the allotrope formation in elemental gallium films. *Mater. Res. Express* **2019**, *6*, 116401. [[CrossRef](#)]
69. Zagorac, D.; Zagorac, J.; Schön, J.C.; Stojanovic, N.; Matovic, B. ZnO/ZnS (hetero)structures: *Ab initio* investigations of polytypic behavior of mixed ZnO and ZnS compounds. *Acta Crystallogr. B* **2018**, *74*, 628–642. [[CrossRef](#)]
70. Zagorac, D.; Zagorac, J.; Pejić, M.; Matović, B.; Schön, J.C. Band Gap Engineering of Newly Discovered ZnO/ZnS Polytypic Nanomaterials. *Nanomaterials* **2022**, *12*, 1595. [[CrossRef](#)]
71. Pejić, M.; Zagorac, D.; Zagorac, J.; Matović, B.; Schön, J.C. Structure prediction via global energy landscape exploration of the ternary rare-earth compound LaOI. *Z. Anorg. Allg. Chem.* **2022**, *648*, e202200308. [[CrossRef](#)]
72. Schön, J.C. Energy landscapes in inorganic chemistry. In *Comprehensive Inorganic Chemistry III*; Poepelmeier, K., Reedijk, J., Eds.; Elsevier: Amsterdam, The Netherlands, 2023; pp. 262–392.

**Disclaimer/Publisher's Note:** The statements, opinions and data contained in all publications are solely those of the individual author(s) and contributor(s) and not of MDPI and/or the editor(s). MDPI and/or the editor(s) disclaim responsibility for any injury to people or property resulting from any ideas, methods, instructions or products referred to in the content.